Original Article

Dynamic characterization of vascular response and treatment in oral traumatic ulcer in mice via photoacoustic imaging

Xiaoyu Miao[1#], Rui Ma[2#], Jiayi Li[1], Wenran You[1], Kaini He[1], Fan Meng[3], Fengbing He[3], Zicong Li[1], Xi Chen[1], Hui Lin[1], Jian Zhang[3*], Xinhong Wang[1*]

[1]Department of Oral Mucosal Diseases, School and Hospital of Stomatology, Guangdong Engineering Research Center of Oral Restoration and Reconstruction, Guangzhou Key Laboratory of Basic and Applied Research of Oral Regenerative Medicine, Guangzhou Medical University, Guangzhou, China; [2]MOE Key Laboratory of Laser Life Science & Institute of Laser Life Science, College of Biophotonics, South China Normal University, Guangzhou, China; [3]Qingyuan People's Hospital, the Sixth Affiliated Hospital of Guangzhou Medical University, School of Biomedical Engineering, Guangzhou Medical University, Guangzhou, China

Contributions: (I) Conception and design: X Wang, J Zhang; (II) Administrative support: X Wang, J Zhang; (III) Provision of study materials or patients: X Wang, J Zhang; (IV) Collection and assembly of data: X Miao, R Ma, J Li, W You, K He, F Meng, F He, Z Li, X Chen; (V) Data analysis and interpretation: X Miao, R Ma; (VI) Manuscript writing: All authors; (VII) Final approval of manuscript: All authors.

[#]These authors contributed equally to this work.

[*]These authors contributed equally to this work as co-corresponding authors.

Correspondence to: Xinhong Wang, MD, PhD. Department of Oral Mucosal Diseases, School and Hospital of Stomatology, Guangdong Engineering Research Center of Oral Restoration and Reconstruction, Guangzhou Key Laboratory of Basic and Applied Research of Oral Regenerative Medicine, Guangzhou Medical University, No. 195 Dongfeng Xi Road, Guangzhou 510182, China. Email: xinhongwang2020@163.com; Jian Zhang, PhD. Qingyuan People's Hospital, the Sixth Affiliated Hospital of Guangzhou Medical University, School of Biomedical Engineering, Guangzhou Medical University, No. 1 Xinzao Road, Guangzhou 511436, China. Email: jianzhang@gzhmu.edu.cn.

Background: Dynamic surveillance of vasculature is essential for evaluating the healing of oral ulcer. Existing techniques used in vascular imaging face limitations, such as inadequate spatial resolution, restricted diagnostic depth, and the necessity of exogenous contrast agents. Therefore, this study aimed to use robust photoacoustic imaging (PAI) for the dynamic monitoring of vascular response during healing and the associated treatment process of oral ulcer.

Methods: Kunming mice (male, 8 weeks old, 31–41 g) were treated with 50% acetic acid for 90 s on the tongue mucosa for induction of oral traumatic ulcer. Mice were randomly divided into three groups (n=12): the control, compound chamomile and lidocaine hydrochloride gel (CCLH), and phycocyanin (PC) groups. PAI was then conducted on days 0, 2, 3, 5, and 7 to obtain vessel parameters of the ulcer area, including vessel intensity, density, mean diameter, maximum diameter, and curvature. Immunohistochemical and hematoxylin and eosin (HE) staining were performed on days 3 and 7 to assess microvessel density and inflammation score. The ulcer healing rate and body weight changes were evaluated for clinical observation.

Results: Beginning on the second day after ulcer induction, there was a progressive increase over time in blood intensity and vessel parameters, including vascular density and diameter. On day 7, the CCLH and PC groups demonstrated significantly higher measures than did the control group in terms of blood intensity ($P<0.05$ and $P<0.01$), vascular density (both P values <0.05), mean diameter (both P values <0.01), and maximum diameter ($P<0.01$ and $P<0.05$). Vessel curvature in the two treatment groups exhibited no significant differences compared to that in the control group (both P values >0.05). The effects of vascular morphological changes were further supported by the histological and clinical outcomes. On day 7, compared to that of the control group, the level of microvessel density was significantly higher in both the CCLH ($P<0.01$) and PC ($P<0.05$) groups. The histopathological score in PC group was significantly lower

than that of the control group on day 7 (P<0.05). Additionally, compared to that of the control group, the healing rates of the CCLH (P<0.01) and PC groups (P<0.05) were superior on day 7. On day 3, the control group showed more weight loss than did the CCLH (P<0.05) and PC (P<0.01) groups.

Conclusions: These findings indicate that PAI is a valuable strategy for the dynamic and quantitative analysis of vascular alterations in oral traumatic ulcers and support its prospective application in improving clinical treatment.

Keywords: Angiogenesis; oral traumatic ulcer; photoacoustic imaging (PAI); vascular response; phycocyanin (PC)

Submitted Jan 22, 2024. Accepted for publication Apr 26, 2024. Published online Jun 04, 2024.
doi: 10.21037/qims-24-123
View this article at: https://dx.doi.org/10.21037/qims-24-123

Introduction

Oral traumatic ulcer is a common mucosal ailment that manifests as a loss of epithelium and underlying connective tissue (1,2). The healing period for oral mucosal traumatic ulcers is typically between 7 and 14 days. However, insufficient angiogenesis may impede the healing process and lead to chronic wound formation (3). Revascularization is a pivotal vascular event in the proliferative phase of wound healing since it facilitates adequate oxygen and nutrient supply and promotes growth factor secretion in the ulcer site to accelerate the final repair of the mucosal defect (4,5). Other vascular responses such as blood coagulation, vascular leakage, and damage are also crucial processes that affect wound healing (6). Therefore, gaining insights into the spatiotemporal dynamics of these phenomena may facilitate a comprehensive characterization of wound healing progression and the development of effective therapeutic strategies to expedite recovery.

Although the role of the vascular system in ulcer healing has recently attracted increased attention, it nonetheless remains largely underexplored. Several conventional imaging techniques used for detection, including microtomography angiography, confocal microscopy, laser speckle imaging, multiphoton microscopy, and ultrasound imaging, have been limited by insufficient spatial resolution, restricted diagnostic depth, and the need for exogenous contrast agents (7-9). As a result, there is a pressing need for a more robust vascular imaging method that can be used to fully understand the vascular response during the wound healing process. Based on the strong intrinsic optical absorption contrast from hemoglobin, photoacoustic imaging (PAI) enables label-free visualization of vascular structure and function with micron-scale imaging resolution and effective tissue penetration (10-13). In addition, the long-term and real-time tracking ability of PAI can provide dynamic surveillance and assessment of the vascular response. PAI has exhibited promise in an array of biological and clinical applications, including eclampsia, ischemic stroke, myocardial infarction, and obesity (14-17). For example, Petri *et al.* (18) were the first to apply PAI to evaluate the treatment of human foot ulcers, demonstrating that PAI possesses great potential as an auxiliary diagnostic tool and therapeutic intervention in ulcer healing assessment and ulcer care management. The development of small instruments designed specifically for oral use further indicates the enormous potential application value of PAI technology in oral diseases, including oral ulcers (19,20). Furthermore, the use of mouse models mimicking oral ulcers in humans can facilitate more convenient and in-depth monitoring, as mice exhibit a resemblance to humans in terms of oral mucosal structure (21,22). However, literature on the dynamic characterization and quantitative analysis of vasculature changes and of the associated treatment response in oral traumatic ulcer model of mice using PAI is lacking.

Therefore, we conducted a study that employed PAI to evaluate and analyze the changes in blood perfusion and vascular structures in oral traumatic ulcers as well as the associated treatment processes of compound chamomile and lidocaine hydrochloride gel (CCLH) and phycocyanin (PC), which have been extensively researched and reported in wound care and treatment (23-26). The therapeutic effect of the latter in oral ulcers warrants further verification. In addition, we further corroborated the *in vivo* PAI findings with histological and clinical analysis of vessel density and ulcer healing rate. These findings might provide further insight into the vascular responses and application of novel drugs for treating oral ulcers. We present this article in accordance with the ARRIVE

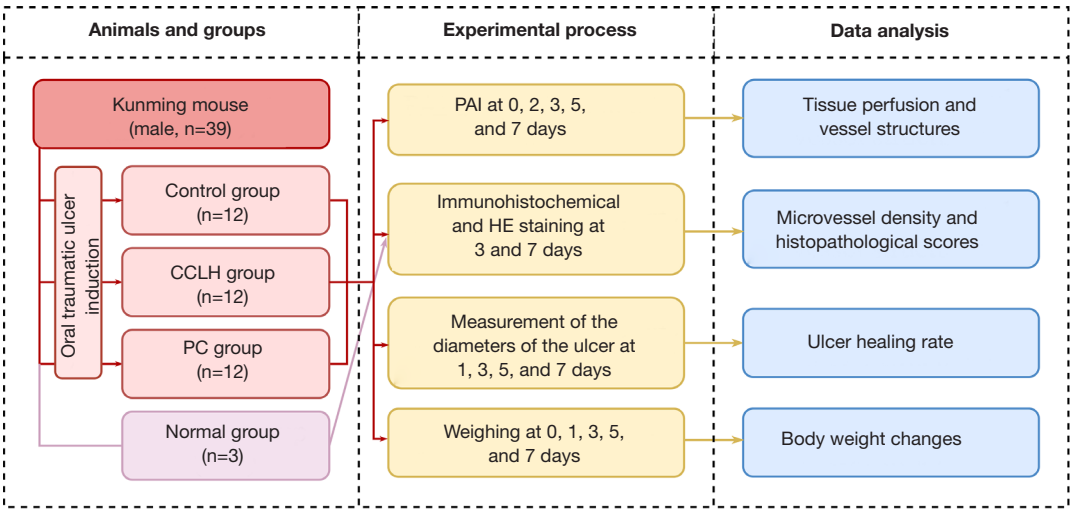

Figure 1 Experimental procedures of the study. Kunming mice were allocated into a control group (n=12), CCLH group (n=12), PC group (n=12), and normal group (n=3). The PAI system was employed on days 0, 2, 3, 5, and 7 to acquire parameters associated with tissue perfusion and vascular structures. Ulcer tissues obtained from mice on days 3 and 7 were subjected to histological analysis. Ulcer area measurements on days 1, 3, 5, and 7 were used to quantify the degree of healing as the ulcer healing rate. The animals' initial weights were recorded at day 0, and subsequent weights were measured at 1, 3, 5, and 7 days after ulceration to assess changes in body weight. CCLH, compound chamomile and lidocaine hydrochloride gel; PC, phycocyanin; PAI, photoacoustic imaging; HE, hematoxylin and eosin.

reporting checklist (available at https://qims.amegroups.com/article/view/10.21037/qims-24-123/rc).

Methods

Animals

This study was approved by the Animal Research Ethics Committee of Guangdong Huawei Testing Co., Ltd. (No. 202306004) and was conducted in compliance with national and institutional guidelines for the care and use of animals. A total of 39 male Kunming mice, aged 8 weeks and weighing 31–41 g, were purchased from Guangdong Huawei Testing Co., Ltd. (Guangzhou, China). The mice, with five animals per cage, were acclimatized for one week under specific pathogen-free (SPF) conditions at a temperature of 22–24 ℃, a relative humidity of 50–70%, and a 12-hour light-dark cycle, with free access to food and water. The sample size was determined based on a previous study (27).

Induction of oral mucosa traumatic ulcer

Mice were anesthetized with 2% pentobarbital sodium. The induction method for oral traumatic ulcers was adapted from Chen *et al.* (28). Briefly, a round plastic tube (3 mm in diameter) filled with cotton balls soaked in 3 mL of 50% acetic acid (Henan Jinmao Medical Technology Co., Ltd., Zhengzhou, China) was pressed into the right dorsal surface of the tongue mucosa for 90 s. An ulcer bed present on the tongue after 24 hours indicated successful model establishment (29). The experimental protocol is shown in *Figure 1*. Random numbers were generated using the "=RAND ()" function in Microsoft Excel (Microsoft Corp., Redmond, WA, USA) to allocate mice into three groups (n=12) (30). In the control group, ulcers were left without any treatment; in the CCLH group, CCLH (Kamistad, STADA Arzneimittel AG, Bad Vilbel, Germany) was applied on the ulcer site of the tongue mucosa twice a day; in the PC group, 200 mg/L of PC solution (Zhejiang Binmei Biotechnology Co., Ltd., Taizhou, China) was administered as the sole source of water. After seven days of treatment, all the mice were euthanized under anesthesia. All experiments were conducted by the same investigator to minimize potential biases. Only the treatment provider was aware of the group allocation during the trial.

PAI system

Figure 2A shows the schematic diagram of the oral

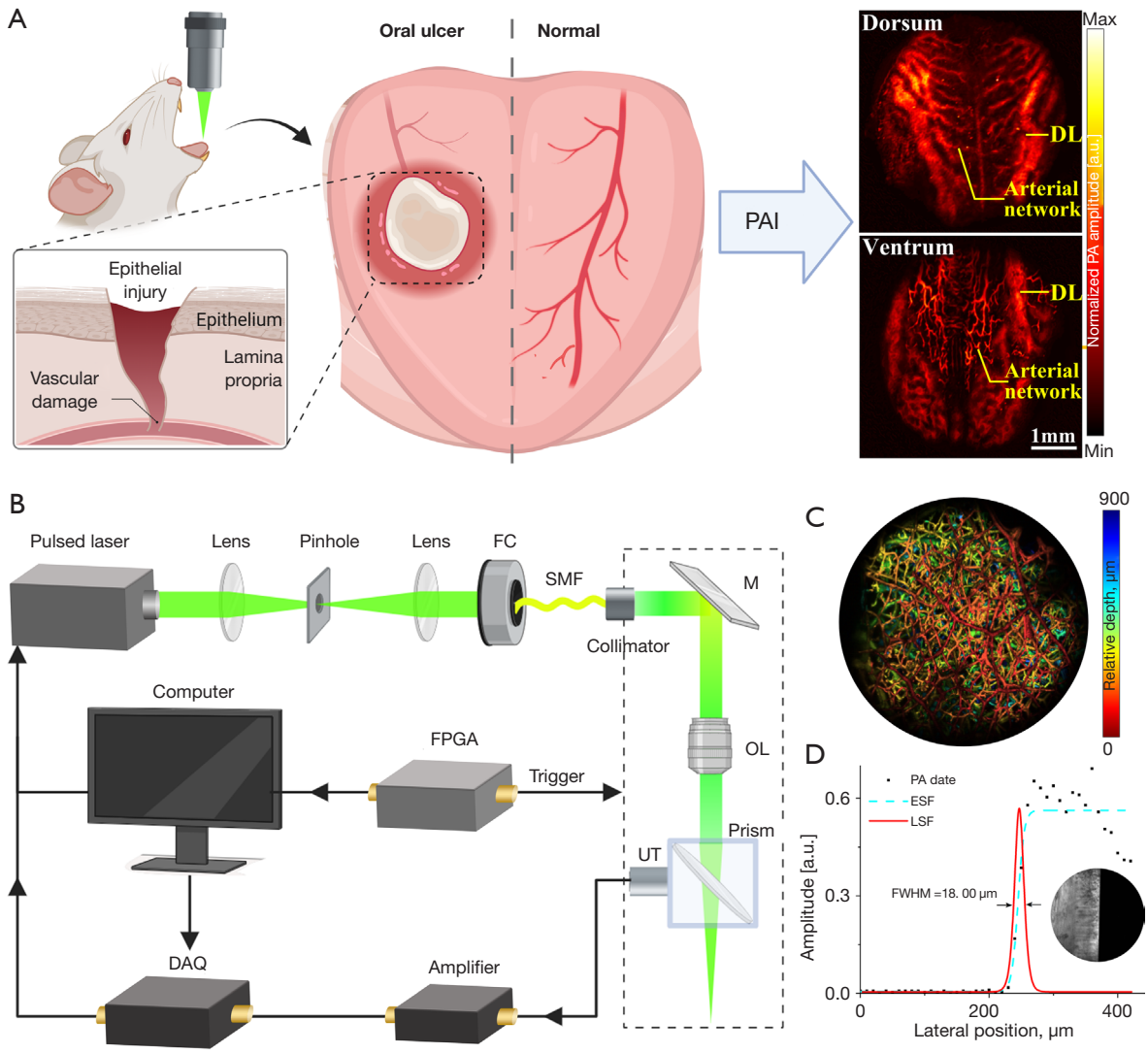

Figure 2 Schematic of oral traumatic ulcer pathology, PAI system, and its imaging principle. (A) Schematic diagram of the oral traumatic ulcer lesion and representative PA images of a healthy mouse tongue from the dorsal and ventral surfaces (created with Biorender.com). (B) Schematic of the PAI system (created with Biorender.com). (C) Images of the multilayer leaf vein. (D) The lateral resolution of the system evaluated with a sharp edge. PAI, photoacoustic imaging; DL, deep lingual artery; FC, fiber coupler; SMF, single-mode fiber; M, mirror; FPGA, field-programmable gate array; OL, objective lens; UT, ultrasonic transducer; DAQ, data acquisition card; PA, photoacoustic; ESF, edge spread function; LSF, line spread function; FWHM, full width at half maximum.

traumatic ulcer model and PAI system used to depict the normal vasculature of the tongue (31). The actual imaging system is shown in Figure S1, and the operating principle of the system is shown in *Figure 2B*. A 532-nm laser (5 ns, 10 kHz) was used and coupled to a single-mode fiber through a fiber coupler. The collimated light was scanned by a fast two-dimensional mirror scanner driven by a field-programmable gate array (FPGA) and focused with an objective lens for photoacoustic (PA) signal excitation. For detecting the PA signals, an ultrasonic transducer with a 15-MHz center frequency and –6-dB fractional bandwidth of over 80% was used and coupled with the imaging area of oral mucosa through medical ultrasound coupling gel. Subsequently, the signals were amplified with an amplifier, digitalized via a data acquisition card, and ultimately stored in a computer. The imaging depth of this PAI system was

900 μm (*Figure 2C*). The lateral and axial resolutions were 18.00 and 140.36 μm, respectively (*Figure 2D*, Figure S2). The traumatic ulcer area of anesthetized mice was scanned with this the system on days 0, 2, 3, 5, and 7 to obtain PA images. Since tissue edema on day 1 reduced the ability of light to penetrate through the tissue, images were not obtained on day 1. A distinct area of vascular interruption after ulcer induction was indicated by a decrease in PA signals and defined as the region of interest (ROI; 1 mm × 1 mm) (32). The surrounding blood vessels and branch points remained relatively intact and exhibited stable morphological and distribution characteristics over time, serving as feature points. Comparison of these feature points at different stages ensured that the positions of ROIs remained consistent relative to these points throughout the entire experiment (33).

Image processing and quantification of vascular parameters

The original PA images underwent filtering and enhancement to improve blood vessel contrast and emphasize the vascular structure. Subsequently, the blood vessels were segmented through threshold processing. Vascular skeletons were then extracted via a multistencil fast marching algorithm. Based on the original and processed images, the vessel parameters including vessel intensity, density, mean diameter, maximum diameter, and curvature can be computed. The vessel intensity was extracted by fitting a normalized Gaussian curve to the cross-sectional profile of the vessel along the y direction. The vessel density can be estimated as the ratio of the vessel pixel number to the total pixel number. For each point of the vascular skeleton, the vessel diameter was calculated as the Euclidean distance between the edge lines orthogonal to the centerline (34). Vessel curvature was computed as the ratio of the actual path length (arc length) over the linear distance (chord length) between a pixel point and its neighboring point along the same branch, while curvature at every pixel of the vessel was summed. All vessel parameters were normalized to the baseline values obtained on day 0. To clarify the quantitative results, three-dimensional visualization was performed based on PA data using the Amira software platform (Thermo Fisher Scientific, Waltham, MA, USA). A green-dotted cube was used to highlight the three-dimensional images of ROIs, with a total volume of 1×1×1 mm^3. Representative cross-sectional PA images were segmented manually to further illustrate the healing process in the PC group.

Histological analysis of oral traumatic ulcer

The animals were euthanized using phenobarbital on days 3 and 7. The normal group (n=3) comprised of mice without oral traumatic ulcers, was used in immunohistochemistry. The excised ulcer tissues were preserved in 4% paraformaldehyde solution and then embedded in paraffin and sectioned into 4-μm slices. Immunohistochemical staining was performed according to normal procedures. Briefly, the samples were incubated overnight at 4 ℃ with primary antibodies against CD34 (dilution 1:2,000; lot: ab81289; Abcam, Cambridge, UK) and then exposed to the secondary antibodies and substrate. The images of stained sections were obtained with a Leica GT450 scanner (Leica Microsystems, Wetzlar, Germany). Some sections for immunohistochemical staining were excluded from the study, as they did not contain ulcer tissue or tissue after ulcer healing. The microvessel density was then assessed through CD34 staining following a previously described protocol (35). This was followed by hematoxylin and eosin (HE) staining, based on which an inflammation score from 0 to 4 (36) was determined by two pathologists in a blinded manner.

Clinical evaluation

The animals were weighed at day 0 (initial weight) and then weighed at 1, 3, 5, and 7 days (final weight) after ulceration. The body weight was evaluated according to the following formula: weight changes (g) = (final weight – initial weight). On days 1, 3, 5, and 7, we measured the ulcer area by a ruler with 1-mm precision and obtained the ulcer area as follows: ulcer area (mm^2) = ($D \times d \times \pi/4$), where D is the larger diameter, and d is the smaller diameter. The degree of healing was expressed as the ulcer healing rate, which was calculated as follows: ulcer healing rate (%) = ($[A_1 - A_t]/A_1 \times 100\%$), where A_1 is the initial ulcer area on day 1, and A_t is the ulcer area at the specific time of observation (28). No adverse events were observed in the mice during this study.

Statistical analysis

Data were analyzed using SPSS version 26.0 (IBM Corp., Armonk, NY, USA). All results are presented as the mean ± standard deviation (SD). Statistical comparisons of groups were conducted using one-way analysis of variance

(ANOVA) with the least significant difference (LSD) post hoc analysis when there was homogeneity of variance. Otherwise, the Dunnett T3 method was used. Statistical significance was set at $P \leq 0.05$.

Results

In vivo PAI monitoring of changes in blood perfusion during ulcer healing

To understand the dynamic blood vessel responses after traumatic ulcer induction, PA images were obtained at 0, 2, 3, 5, and 7 days (*Figure 3*). PA signals often reflect information about the hemodynamics including tissue perfusion; therefore, distinct hemorrhaging, vascular recovery, and injury could be visualized in three-dimensional PA images (*Figure 3B*), as demonstrated in *Figure 3A*. On the second day after ulcer induction, the lingual vessels at the ulcer area were absent to differing degrees in three groups, and PA signals were weakened due to vascular damage. Subsequently, there hemorrhage was apparent in the PA images of all three groups, which was indicated by diffuse spot-like signals, which were particularly pronounced in the control group. The intense hemorrhaging led to strong PA signals, which was calculated as the vessel signal during processing. Therefore, no significant differences were found in blood intensity among groups on day 3, with 66.48%±11.19% in the control group, 73.56%±12.54% in the CCLH group, and 73.73%±7.03% in the PC group (all P values >0.05) until the hemorrhage had receded. These bleeding signals gradually decreased over time and were replaced by reperfusion of blood vessels at each corresponding time point, eventually disappearing. In the CCLH and PC groups, the vessel intensity gradually increased as the ulcer healed and by day 7, had nearly returned to baseline levels of 90.82%±8.15% and 96.57%±9.68%, respectively. Ultimately, both the CCLH [95% confidence interval (CI): 1.97–28.82; P=0.027] and PC (95% CI: 7.72–34.58; P=0.004) groups experienced greater blood circulation than did the control group. Differences in microvascular morphology delineated in close-ups of representative ROIs further confirmed this finding. Several collateral vessels barely visible and poorly perfused before ulcer formation were recruited in CCLH and PC groups on day 7. By contrast, the recovery of the vasculature in the control group was less significant.

In vivo PAI characterization of alterations in vascular structures during ulcer healing

To gain quantitative insight into the dynamic alterations of vessel structures during ulcer healing, the vascular parameters (density, mean diameter, maximum diameter, and curvature) were obtained from mice before and after traumatic ulcer induction (*Figure 4A*,*4B*). It was observed that these parameters immediately decreased on day 2. Subsequently, vascular density and mean and maximum diameter displayed an overall upward trend with time. The control group showed a slight increase, while the CCLH and PC groups exhibited a greater increase, nearly returning to baseline levels by the seventh day. On day 7, compared to the control group, the CCLH and PC groups demonstrated significantly higher vascular density (CCLH group: 92.25%±22.26%, 95% CI: 2.03–54.99, P=0.037; PC group: 97.12%±26.46%, 95% CI: 6.91–59.87, P=0.017), mean diameter (CCLH group: 92.71%±26.92%, 95% CI: 9.50–58.89, P=0.009; PC group: 102.92±16.08, 95% CI: 19.71–69.10, P=0.002), and maximum diameter (CCLH group: 100.18%±17.88%, 95% CI: 18.80–70.77, P=0.002; PC group: 87.05%±21.33%, 95% CI: 1.70–61.62, P=0.039). Vessel curvature remained relatively constant over time and exhibited no significant differences among the control (93.08%±6.53%), CCLH (104.30%±7.50%), and PC (98.42%±8.36%) groups (all P values >0.05). Three-dimensional volumetric PA images further depicted the increased complexity of the vascular network in the healing process of mice treated with PC, including enhanced vascular density and enlarged diameters (*Figure 4C*,*4D*). Finally, the restored vasculature with prominent morphologies at both the local and overall levels could be clearly observed after 7-day PC treatment.

Histological changes in vascularization and inflammation in the ulcer site

We further analyzed the vessel density in the ulcer tissue using CD34 staining *(Figure 5A*,*5B*). On the third day, the level of microvessel density in the control and CCLH groups was lower than that of the normal group, measuring 90.22±69.17 (95% CI: 99.44–432.78; P=0.007) and 129.67±61.59 (95% CI: 78.77–532.34; P=0.019), respectively. However, the microvessel density of the PC group was 299.33±153.24, showing no significant

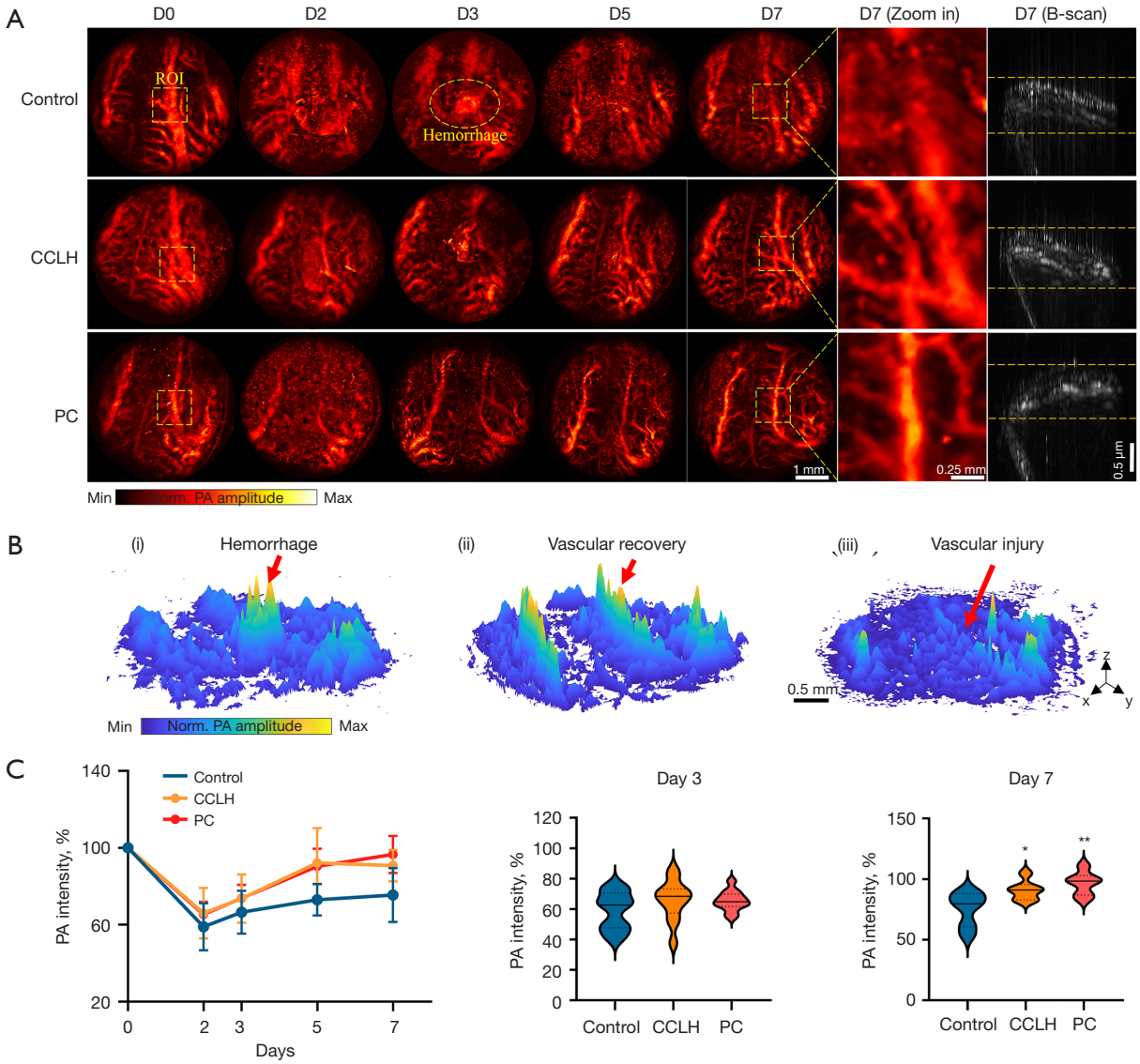

Figure 3 *In vivo* PAI monitoring of changes in blood perfusion during ulcer healing. (A) Longitudinal visualization of the vascular system in the tongue mucosa before and after traumatic ulcer modeling. The dotted rectangles indicate the ROIs, and the dotted ellipse indicates hemorrhage. (B) Representative PA images according to (A) show (I) hemorrhage on the third day in the control group, (II) vascular recovery on the seventh day in the PC group, and (III) delayed vascular recovery on the seventh day in the control group. (C) Quantification of the normalized PA signal intensity during 7-day monitoring among different groups (n=12 on days 0, 2, and 3; n=6 on days 5 and 7). *, P<0.05; **, P<0.01. CCLH, compound chamomile and lidocaine hydrochloride gel; PC, phycocyanin; PAI, photoacoustic imaging; ROI, region of interest; PA, photoacoustic.

difference compared to the normal value (P>0.05). On the seventh day, in comparison to that in the control group, the vascular density at the ulcer site was remarkably elevated to 491.58±80.02 in the CCLH group (95% CI: 128.22–459.39; P=0.003) and 396.44±35.88 in the PC group (95% CI: 21.65–375.68; P=0.032). Meanwhile, the blood vessel coverage in the control group was 197.78±167.21, which indicated that it had not yet returned to normal levels (95% CI: 20.99–375.01; P=0.032).

The HE staining demonstrated surface epithelial necrosis and dense neutrophil infiltration in the oral traumatic ulcer tissue of the control group on the third day

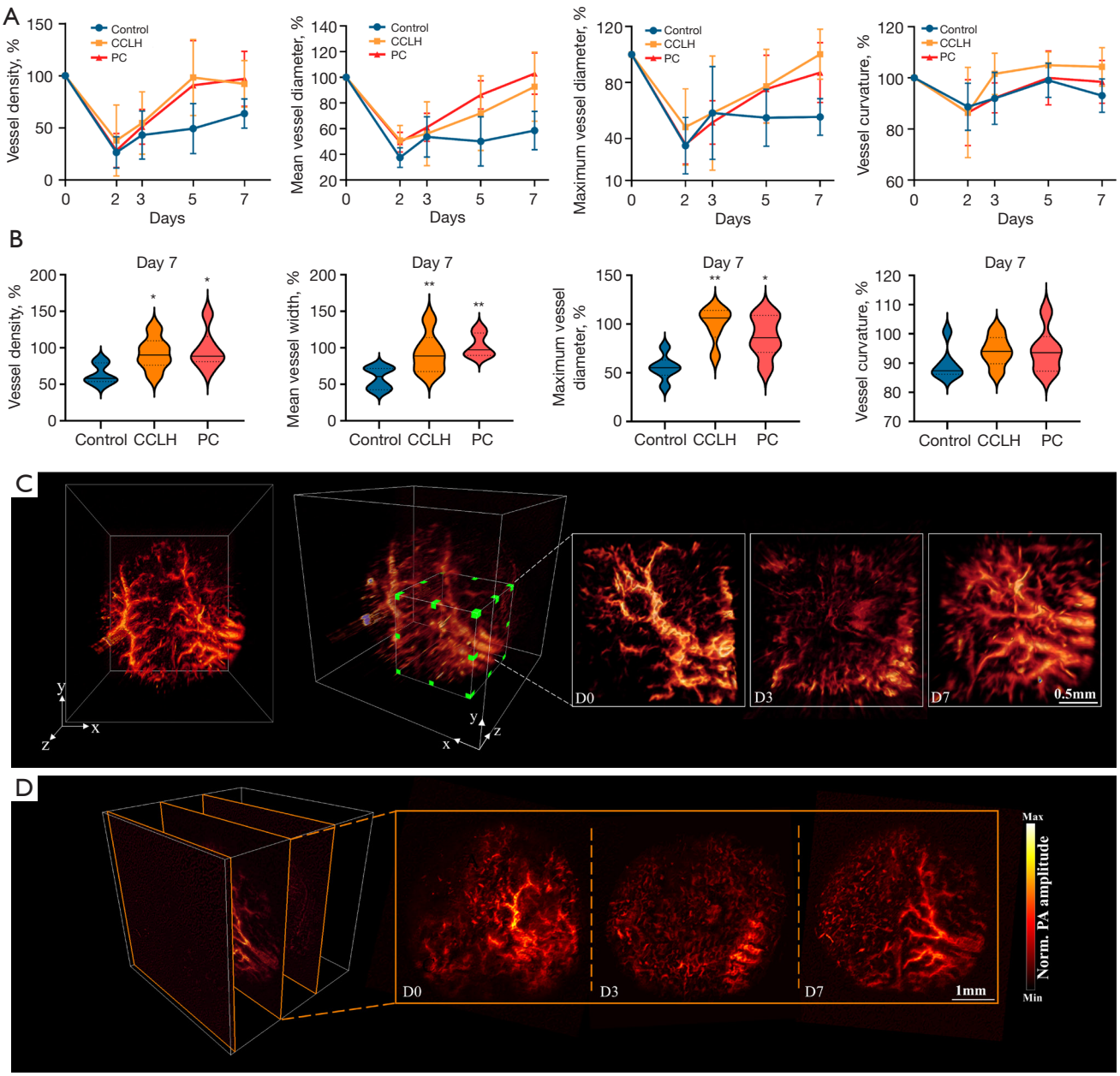

Figure 4 *In vivo* PAI characterization of alterations in vascular structures during ulcer healing. (A) Changes in the vasculature structure of density, mean diameter, maximum diameter, and curvature of the ulcer area over the 7-day monitoring (n=12 on days 0, 2, and 3; n=6 on days 5 and 7). (B) Quantification of vascular alterations on day 7 (n=6). (C) Three-dimensional visualization of vessel structural response treated with PC during 7-day ulcer healing. (D) Representative cross-sectional slices corresponding to the images of (C). *, P<0.05; **, P<0.01. CCLH, compound chamomile and lidocaine hydrochloride gel; PC, phycocyanin; PAI, photoacoustic imaging.

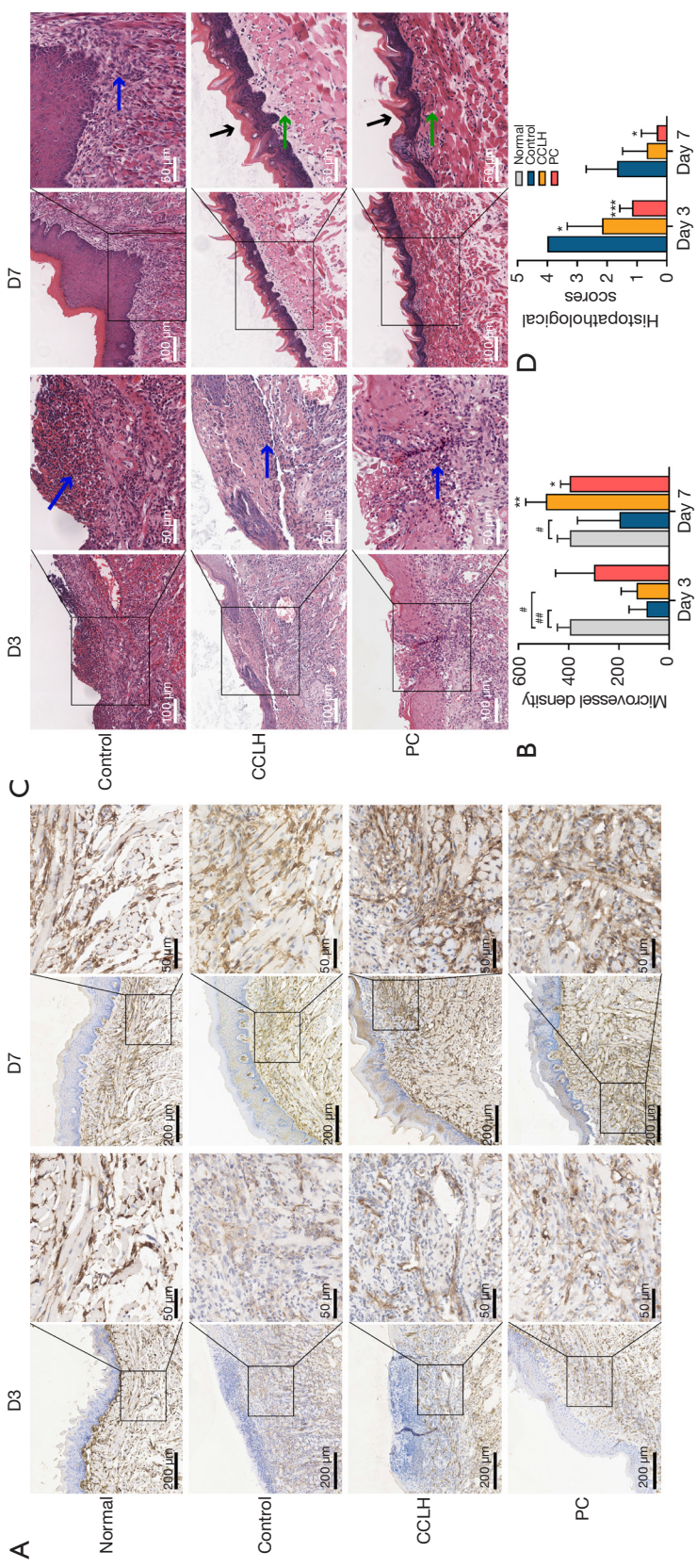

Figure 5 Histological changes in vascularization and inflammation in the ulcer site. (A) Immunohistochemical staining of CD34 expression in ulcer sections in the normal, control, CCLH, and PC groups on days 3 and 7 after traumatic ulcer induction (100×, scale bar =200 μm; 400×, scale bar =50 μm). (B) Quantification of microvessel density from immunohistochemical staining on day 3 (n=3 in the normal group, n=4 in the other groups) and day 7 (n=3). (C) HE staining of oral traumatic ulcers in three groups (200×, scale bar =100 μm; 400×, scale bar =50 μm). Blue arrows indicate infiltrated inflammatory cells, black arrows indicate reepithelization, and green arrows indicate inflammation alleviation. (D) Quantification of the inflammation scores from HE staining on day 3 (n=6) and day 7 (n=6). *, P<0.05; **, P<0.01; ***, P<0.001 (*vs.* control group). #, P<0.05; ##, P<0.01 (*vs.* normal group). CCLH, compound chamomile and lidocaine hydrochloride gel; PC, phycocyanin; HE, hematoxylin and eosin.

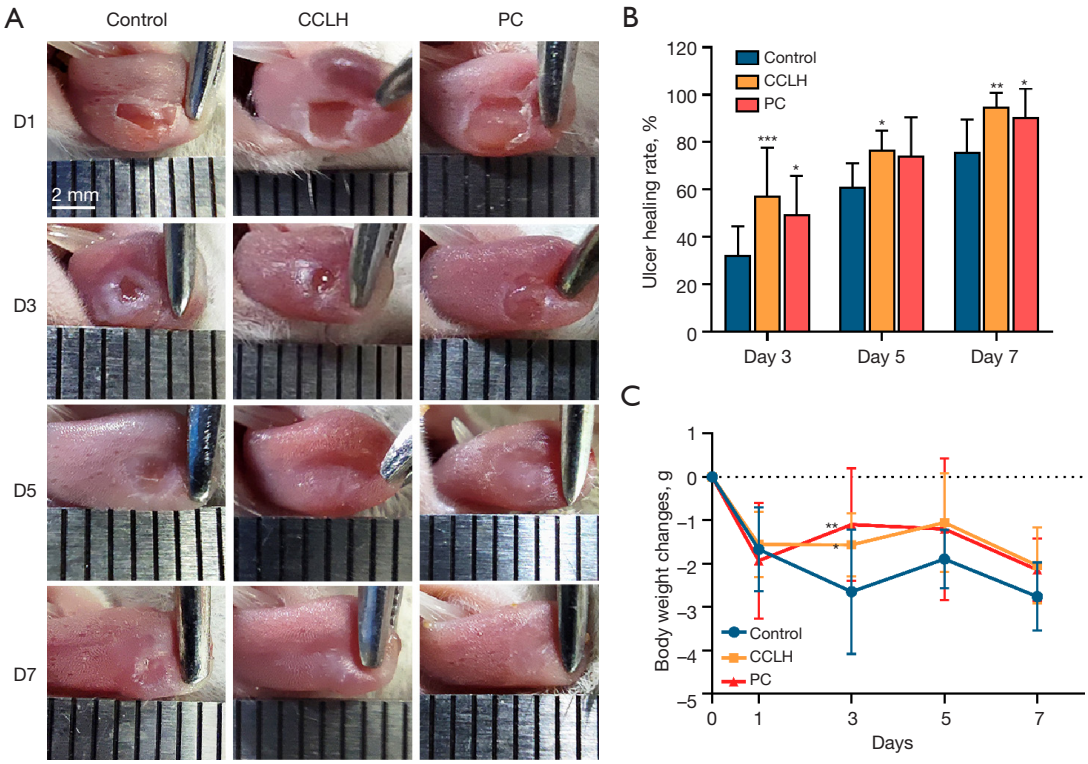

Figure 6 Clinical evaluation of ulcer area and weight changes. (A) Traumatic ulcer healing process under control, CCLH treatment, and PC treatment conditions on days 1, 3, 5, and 7 after traumatic ulcer induction. (B) Quantification of the ulcer healing rate according to macroscopic observation (n=12 on day 3; n=6 on days 5 and 7). (C) Weight changes in three groups at different time points after traumatic ulcer modeling (n=12 on days 0, 1, and 3; n=6 on days 5 and 7). *, P<0.05; **, P<0.01; ***, P<0.001. CCLH, compound chamomile and lidocaine hydrochloride gel; PC, phycocyanin.

(*Figure 5C*,*5D*). Compared to that of the control group, the degree of ulceration and a subepithelial inflammatory activity was milder in the tissue treated with CCLH (95% CI: 0.21–3.46; P=0.032) or PC (95% CI: 2.27–3.40; P<0.001). The histopathological scores were 2.17±1.17 in the CCLH group and 1.17±0.41 in the PC group. On the seventh day, the control group exhibited chronic inflammatory infiltration (mainly lymphocytes) beneath immature epithelial coverage. By contrast, CCLH and PC treatment led to better reepithelization and less inflammation, and the histopathological score of 0.33±0.52 in the PC group was significantly lower than that of the control group on day 7 (95% CI: 0.33–2.34; P=0.013).

Clinical evaluation of ulcer healing rate and weight changes

The healing rate analysis revealed that the traumatic ulcer healed gradually in all groups over time (*Figure 6*). From day 3 to 7, the CCLH group exhibited the highest healing rate, significantly greater than that of the control group. It was 57.50%±19.97% (95% CI: 11.70–38.90%; P<0.001) on day 3, 76.80%±7.85% (95% CI: 1.30–30.15%; P=0.035) on day 5, and 94.83%±6.01% (95% CI: 5.40–32.56%; P=0.009) on day 7. Similarly, the PC group exhibited superior healing rates of 49.58%±16.01% (95% CI: 3.77–30.98%; P=0.014) and 90.52%±11.95% (95% CI: 1.09–28.25%; P=0.036) compared to the control group on the day 3 and day 7, respectively. The weight changes in all groups of mice from day 1 to day 7 were similar. Starting from the third day, the control group of mice showed more weight loss than did the other two groups, but significant differences were only observed on the third day. Weight changes on day 3 were –1.57±0.72 g (95% CI: 0.09–2.07; P=0.033) in the CCLH group and –1.10±1.30 g (95% CI: 0.56–2.53; P=0.003) in the PC group.

Discussion

The process of vascular response is closely related to the progress of wound healing. In this study, we dynamically monitored and evaluated the vascular changes in a mouse oral traumatic ulcer model and evaluated the therapeutic effect of CCLH and PC using PAI. We observed gradually elevated levels of tissue perfusion, vascular density, and diameter in the replacement of the damaged vasculature after ulcer induction during the 7-day monitoring. These observations and evaluations were corroborated by increased microvessel density, reduced inflammation levels, higher healing rates, and body weight gain in histology and clinical performances. Our observations confirmed the capability of PAI in dynamic characterization of the altered tissue perfusion and vascular responses and in the evaluation of therapeutic efficacy.

Vessel intensity indicated by PA signals is related to the total hemoglobin concentration and can be applied to predict tissue perfusion (37). We showed that our system is capable of dynamically visualizing and identifying valuable phenomena at different time points of ulcer healing. The initial disappearance of the vasculature after traumatic ulcer formation can be ascribed to the constricted and occluded arteries caused by the aggregation of platelets and leukocytes. This process, known as hemostasis, typically occurs within the first few days of healing (38). Subsequently, the marked bleeding in control group may be associated with increased microvascular permeability, which exerts a more significant impact than does vascular occlusion and promotes vascular leakage and the thickening of the tissue. The observed reduction in vessel intensity in the control group from day 5 to day 7 suggested delayed vessel perfusion after the subsidence of bleeding. The occurrence of hemorrhage and vessel discontinuities may be linked to the endothelial injury caused by lingering inflammatory cells (39). Research has confirmed that the timely conversion in wound healing from inflammation to proliferation promotes the restoration of the vascular system (4). The reduction of inflammation, especially on the endothelium, might help attenuate leukocyte activation and mitigate the loss of capillary integrity. Ultimately, the increased collateral circulation observed in the CCLH and PC groups may be part of a compensatory mechanism, which promotes hemodynamic redistribution and supports the ulcer site with additional blood supply (40).

The structural differences in the vessels are the result of revascularization, which is a pivotal step in the progression of traumatic ulcer healing (6). In wounds with vigorous healing, the newly formed vascular network is typically created with high tortuosity (5). However, in our study, the curvature parameter reflecting vessel tortuosity exhibited only a weak upward trend over time and seemed unaffected by treatment. A possible explanation for this observation is that large vessels are rather smooth compared to the coiled capillaries (41,42). When the measuring region covers the main vessels, the variation of vessel tortuosity may no longer be apparent. We further observed that the restored blood vessels particularly densified and widened in two drug-treated groups, marking the activation of an autoimmune response to recruit pre-existing microvessels and produce neocapillaries (43). These results were verified again with increased vessel density counts reflected in the CD34 expression in our study, as CD34 is a specific endothelial cell marker for neovascularization (35). The perfused microcirculation network provides greater tissue perfusion, which satisfies the demand for oxygen delivery and nutritional supply for ulcer reconstruction (4). In our study, the histological and clinical analysis of inflammatory alleviation, ulcer healing acceleration, and weight gain further confirmed the functions of the recovered vessel network in ulcer healing. Therefore, the vascular responses characterized in the PAI system can not only exhibit physiological relevance but also contribute to further screening of medications that are effective in enhancing oral traumatic ulcer healing via the restoration of blood supply.

Currently, the main treatment strategies for oral ulcers include anti-inflammatory agents, topical corticosteroids, local analgesics and antibiotics (1). Given the issues of drug resistance and side effects associated with conventional medications, natural compounds derived from plants may help mitigate these shortcomings and potentially serve as powerful candidates for medicines. PC is a water-soluble photosynthetic pigment purified from the *Spirulina platensis* (44). In our study, PC was found to increase tissue perfusion and promote the formation of a densified and widened vasculature in the ulceration site. These findings were corroborated by a weakened inflammatory response in PC treatment, which confirmed the possibility of alleviating inflammation in the process of vascular recovery. Similarly, recent reports have demonstrated the merits of PC in restoring ischemic tissue perfusion and protecting the vasculature from damage (45,46). PC can induce the expression of vascular endothelial growth factor A in hypoperfused brain tissue, which is a key gene involved in the initiation of angiogenesis. Meanwhile, PC exerts

an endothelial protective effect against cardiovascular diseases mediated via antioxidant and anti-inflammatory activity, which leads to depressed levels of reactive oxygen species and apoptosis-inducing factors (47,48). Our study indicated that the development of microcirculation notably accelerated ulcer healing with PC treatment, which further confirms the contribution of a well-developed vascular system to wound recovery. Additionally, experimental evidence has demonstrated that PC also enhances wound closure via the stimulation of growth factor secretion, fibroblast proliferation, and collagen synthesis (49,50). These properties jointly achieve the possibility of adequate development of well-healed ulcers. PC is the main active component of *Spirulina platensis*, whose clinical application was found to improve oral ulcer healing compared to aloe vera (51). However, a scientific evaluation of the effects of PC on oral traumatic ulcers and vascular changes during ulcer healing has yet to be conducted. Our study not only confirmed prior observations concerning PC's role in wound healing but also offered novel perspectives on its impact on the evolution of blood perfusion and vessel structures during the ulcer healing process.

Although our study has demonstrated the feasibility of PAI, there are still certain limitations that need to be addressed. With a single wavelength at 532 nm, the PAI system is limited to obtaining vascular information solely based on the absorbance of hemoglobin. We are expanding the PA microscopy to incorporate dual wavelengths, which will enable us to derive functional parameters for oxygen saturation in the mouse model of oral traumatic ulcer in our upcoming research.

Conclusions

Using *in vivo* dynamic PAI technology, this study examined the vascular response in blood perfusion and structures of oral traumatic ulcers and the ulcer-healing efficacy of CCLH and PC. We observed gradual increases in tissue perfusion, vascular density, and diameter associated with the replacement of the damaged vasculature after ulcer induction during the 7-day monitoring, particularly under the administration of CCLH and PC. The effects of recovered microvasculature assessed by PAI were further verified in histological and clinical evaluations, which revealed increased microvessel density, inflammation alleviation, ulcer area reduction, and body weight gain. These findings not only underscore the clinical potential of PAI in assessing vascular responses for the pharmacological treatment of oral traumatic ulcers but also pave the way for exploring novel therapeutic and preventive approaches targeting vascular dynamics in oral traumatic ulcers.

Acknowledgments

Funding: This work was supported by the National Key R&D Program of China (No. 2022YFC2304205), the Guangzhou Municipal Science and Technology Bureau (No. 2024A03J0138), and the Plan on Enhancing Scientific Research in Guangzhou Medical University (No. 02-408-240603131062).

Footnote

Reporting Checklist: The authors have completed the ARRIVE reporting checklist. Available at https://qims.amegroups.com/article/view/10.21037/qims-24-123/rc

Conflicts of Interest: All authors have completed the ICMJE uniform disclosure form (available at https://qims.amegroups.com/article/view/10.21037/qims-24-123/coif). The authors have no conflicts of interest to declare.

Ethical Statement: The authors are accountable for all aspects of the work in ensuring that questions related to the accuracy or integrity of any part of the work are appropriately investigated and resolved. This study was approved by the Animal Research Ethics Committee of Guangdong Huawei Testing Co., Ltd. (No. 202306004) and was conducted in compliance with national and institutional guidelines for the care and use of animals.

References

1. Bilodeau EA, Lalla RV. Recurrent oral ulceration: Etiology, classification, management, and diagnostic algorithm. Periodontol 2000 2019;80:49-60.

2. Fitzpatrick SG, Cohen DM, Clark AN. Ulcerated Lesions of the Oral Mucosa: Clinical and Histologic Review. Head Neck Pathol 2019;13:91-102.
3. Shi Z, Yao C, Shui Y, Li S, Yan H. Research progress on the mechanism of angiogenesis in wound repair and regeneration. Front Physiol 2023;14:1284981.
4. Landén NX, Li D, Ståhle M. Transition from inflammation to proliferation: a critical step during wound healing. Cell Mol Life Sci 2016;73:3861-85.
5. Veith AP, Henderson K, Spencer A, Sligar AD, Baker AB. Therapeutic strategies for enhancing angiogenesis in wound healing. Adv Drug Deliv Rev 2019;146:97-125.
6. Peña OA, Martin P. Cellular and molecular mechanisms of skin wound healing. Nat Rev Mol Cell Biol 2024. [Epub ahead of print]. doi: 10.1038/s41580-024-00715-1.
7. Nishimiya K, Matsumoto Y, Shimokawa H. Recent Advances in Vascular Imaging. Arterioscler Thromb Vasc Biol 2020;40:e313-21.
8. Margolis R, Merlo B, Chanthavisay D, Chavez C, Trinh B, Li J. Comparison of micro-CT image enhancement after use of different vascular casting agents. Quant Imaging Med Surg 2024;14:2568-79.
9. Wang M, Singh R, Zhang W, Orringer JS, Paulus YM, Yang X, Wang X. Cutaneous Hypervascularization Treatment Using Photo-Mediated Ultrasound Therapy. JID Innov 2023;3:100237.
10. Ma H, Cheng Z, Wang Z, Qiu H, Shen T, Xing D, Gu Y, Yang S. Quantitative and anatomical imaging of dermal angiopathy by noninvasive photoacoustic microscopic biopsy. Biomed Opt Express 2021;12:6300-16.
11. Wang Z, Yang F, Ma H, Cheng Z, Zhang W, Xiong K, Shen T, Yang S. Bifocal 532/1064 nm alternately illuminated photoacoustic microscopy for capturing deep vascular morphology in human skin. J Eur Acad Dermatol Venereol 2022;36:51-9.
12. Zhang W, Ma H, Cheng Z, Wang Z, Zhang L, Yang S. Miniaturized photoacoustic probe for in vivo imaging of subcutaneous microvessels within human skin. Quant Imaging Med Surg 2019;9:807-14.
13. Xu Z, Zhang W, Quesada C, Wang X, Fabiilli M. Longitudinal Monitoring of Angiogenesis in a Murine Window Chamber Model In Vivo. Tissue Eng Part C Methods 2024;30:93-101.
14. Cao R, Li J, Zhang C, Zuo Z, Hu S. Photoacoustic microscopy of obesity-induced cerebrovascular alterations. Neuroimage 2019;188:369-79.
15. Lawrence DJ, Bayer CL. Photoacoustic imaging provides an in vivo assessment of the preeclamptic placenta remodeling and function in response to therapy. Placenta 2022;126:46-53.
16. Zhang Y, Chen X, Liu L, Tian J, Hao L, Ran HT. Photoacoustic Imaging of Myocardial Infarction Region Using Non-Invasive Fibrin-Targeted Nanoparticles in a Rat Myocardial Ischemia-Reperfusion Model. Int J Nanomedicine 2021;16:1331-44.
17. Yang X, Chen YH, Xia F, Sawan M. Photoacoustic imaging for monitoring of stroke diseases: A review. Photoacoustics 2021;23:100287.
18. Petri M, Stoffels I, Griewank K, Jose J, Engels P, Schulz A, Pötzschke H, Jansen P, Schadendorf D, Dissemond J, Klode J. Oxygenation Status in Chronic Leg Ulcer After Topical Hemoglobin Application May Act as a Surrogate Marker to Find the Best Treatment Strategy and to Avoid Ineffective Conservative Long-term Therapy. Mol Imaging Biol 2018;20:124-30.
19. Huang B, Wong TTW. Review of low-cost light sources and miniaturized designs in photoacoustic microscopy. J Biomed Opt 2024;29:S11503.
20. Pan Z, Zhang X, Xie W, Cui J, Wang Y, Zhang B, Du L, Zhai W, Sun H, Li Y, Li D. Revisited and innovative perspectives of oral ulcer: from biological specificity to local treatment. Front Bioeng Biotechnol 2024;12:1335377.
21. Toma AI, Fuller JM, Willett NJ, Goudy SL. Oral wound healing models and emerging regenerative therapies. Transl Res 2021;236:17-34.
22. Yang M, Chen X, Cheng C, Yan W, Guo R, Wang Y, Zhang H, Chai J, Cheng Y, Zhang F. Cucurbitacin B induces ferroptosis in oral leukoplakia via the SLC7A11/mitochondrial oxidative stress pathway. Phytomedicine 2024;129:155548.
23. Dranseikienė D, Balčiūnaitė-Murzienė G, Karosienė J, Morudov D, Juodžiukynienė N, Hudz N, Gerbutavičienė RJ, Savickienė N. Cyano-Phycocyanin: Mechanisms of Action on Human Skin and Future Perspectives in Medicine. Plants (Basel) 2022;11:1249.
24. Bannu SM, Lomada D, Gulla S, Chandrasekhar T, Reddanna P, Reddy MC. Potential Therapeutic Applications of C-Phycocyanin. Curr Drug Metab 2019;20:967-76.
25. Sah A, Naseef PP, Kuruniyan MS, Jain GK, Zakir F, Aggarwal G. A Comprehensive Study of Therapeutic Applications of Chamomile. Pharmaceuticals (Basel) 2022.
26. Mir B, Bakhtawar, Naz S, Uroos M, Ali B, Sharif F. Pharmaceutical applications of lidocaine-based ionic liquids – A remarkable innovation in drug delivery. J Mol

Liq 2024;397:124052.
27. Festing MF, Altman DG. Guidelines for the design and statistical analysis of experiments using laboratory animals. ILAR J 2002;43:244-58.
28. Chen P, Yao H, Su W, He Y, Cheng K, Wang Y, Peng W, Li P. Sleep deprivation worsened oral ulcers and delayed healing process in an experimental rat model. Life Sci 2019;232:116594.
29. Luo H, Yu Y, Liang M, Huang Z, Jiang H, Wang Y, Qi J. Efficacy identification and active compounds screening of topically administration of Scutellaria Radix in oral ulcer. J Chromatogr B Analyt Technol Biomed Life Sci 2023;1215:123571.
30. Xiong Y, Xin Y, Liu F, Li W, Liu Y, Zhu J. Efficacy of shear wave dispersion imaging for viscoelastic assessment of the liver in acute graft-versus-host disease rats. Quant Imaging Med Surg 2022;12:5044-55.
31. Dumitru CC, Vrapciu AD, Rusu MC. The Diversity of the Linguofacial Trunk. Medicina (Kaunas) 2024;60:291.
32. Sun N, Bruce AC, Ning B, Cao R, Wang Y, Zhong F, Peirce SM, Hu S. Photoacoustic microscopy of vascular adaptation and tissue oxygen metabolism during cutaneous wound healing. Biomed Opt Express 2022;13:2695-706.
33. Zhang J, Sun X, Li H, Ma H, Duan F, Wu Z, Zhu B, Chen R, Nie L. In vivo characterization and analysis of glioblastoma at different stages using multiscale photoacoustic molecular imaging. Photoacoustics 2023;30:100462.
34. Zhao Y, Li T, Guo H, Hu R, Xi L. Long-term assessment of cutaneous inflammation and treatment using optical resolution photoacoustic microscopy. Biomed Opt Express 2023;14:4775-89.
35. Kataria SP, Malik S, Yadav R, Kapil R, Sen R. Histomorphological and Morphometric Evaluation of Microvessel Density in Nodal Non-Hodgkin Lymphoma Using CD34 and CD105. J Lab Physicians 2021;13:22-8.
36. Oliveira BV, Barros Silva PG, Nojosa Jde S, Brizeno LA, Ferreira JM, Sousa FB, Mota MR, Alves AP. TNF-alpha expression, evaluation of collagen, and TUNEL of Matricaria recutita L. extract and triamcinolone on oral ulcer in diabetic rats. J Appl Oral Sci 2016;24:278-90.
37. Park B, Oh D, Kim J, Kim C. Functional photoacoustic imaging: from nano- and micro- to macro-scale. Nano Converg 2023;10:29.
38. Nurden AT. Molecular basis of clot retraction and its role in wound healing. Thromb Res 2023;231:159-69.
39. Kim YW, West XZ, Byzova TV. Inflammation and oxidative stress in angiogenesis and vascular disease. J Mol Med (Berl) 2013;91:323-8.
40. Bekeny JC, Alfawaz A, Day J, Naz I, Attinger CE, Fan KL, Evans KK, Akbari CM. Indirect Endovascular Revascularization via Collaterals: A New Classification to Predict Wound Healing and Limb Salvage. Ann Vasc Surg 2021;73:264-72.
41. Reif R, Qin J, An L, Zhi Z, Dziennis S, Wang R. Quantifying optical microangiography images obtained from a spectral domain optical coherence tomography system. Int J Biomed Imaging 2012;2012:509783.
42. Guo Z, Li Z, Deng Y, Chen SL. Photoacoustic microscopy for evaluating a lipopolysaccharide-induced inflammation model in mice. J Biophotonics 2019;12:e201800251.
43. Carmeliet P, Jain RK. Molecular mechanisms and clinical applications of angiogenesis. Nature 2011;473:298-307.
44. Ashaolu TJ, Samborska K, Lee CC, Tomas M, Capanoglu E, Tarhan Ö, Taze B, Jafari SM. Phycocyanin, a super functional ingredient from algae; properties, purification characterization, and applications. Int J Biol Macromol 2021;193:2320-31.
45. Marín-Prida J, Pavón-Fuentes N, Llópiz-Arzuaga A, Fernández-Massó JR, Delgado-Roche L, Mendoza-Marí Y, Santana SP, Cruz-Ramírez A, Valenzuela-Silva C, Nazábal-Gálvez M, Cintado-Benítez A, Pardo-Andreu GL, Polentarutti N, Riva F, Pentón-Arias E, Pentón-Rol G. Phycocyanobilin promotes PC12 cell survival and modulates immune and inflammatory genes and oxidative stress markers in acute cerebral hypoperfusion in rats. Toxicol Appl Pharmacol 2013;272:49-60.
46. Xu FH, Qiu YZ, Zhang Y, Yang FH, Ji MM, Liu KC, Jin M, Zhang SS, Li B. The molecular mechanism of three novel peptides from C-phycocyanin alleviates MPTP-induced Parkinson's disease-like pathology in zebrafish. Food Funct 2023;14:6157-71.
47. Li B, Chu XM, Xu YJ, Yang F, Lv CY, Nie SM. CD59 underlines the antiatherosclerotic effects of C-phycocyanin on mice. Biomed Res Int 2013;2013:729413.
48. Rojas-Franco P, Garcia-Pliego E, Vite-Aquino AG, Franco-Colin M, Serrano-Contreras JI, Paniagua-Castro N, Gallardo-Casas CA, Blas-Valdivia V, Cano-Europa E. The Nutraceutical Antihypertensive Action of C-Phycocyanin in Chronic Kidney Disease Is Related to the Prevention of Endothelial Dysfunction. Nutrients 2022;14:1464.
49. Fernandes R, Campos J, Serra M, Fidalgo J, Almeida H, Casas A, Toubarro D, Barros AIRNA. Exploring the Benefits of Phycocyanin: From Spirulina Cultivation to Its Widespread Applications. Pharmaceuticals (Basel)

2023;16:592.
50. Ikeda IK, Sydney EB, Sydney ACN. Potential application of Spirulinain dermatology. J Cosmet Dermatol 2022;21:4205-14.
51. Patil S, Al-Zarea BK, Maheshwari S, Sahu R. Comparative evaluation of natural antioxidants spirulina and aloe vera for the treatment of oral submucous fibrosis. J Oral Biol Craniofac Res 2015;5:11-5.

Cite this article as: Miao X, Ma R, Li J, You W, He K, Meng F, He F, Li Z, Chen X, Lin H, Zhang J, Wang X. Dynamic characterization of vascular response and treatment in oral traumatic ulcer in mice via photoacoustic imaging. Quant Imaging Med Surg 2024;14(7):4333-4347. doi: 10.21037/qims-24-123

